ChemComm



COMMUNICATION

View Article Online



Cite this: DOI: 10.1039/d0cc04563b

Received 2nd July 2020, Accepted 4th August 2020

DOI: 10.1039/d0cc04563b

rsc.li/chemcomm

Bimetallic iron—tin catalyst for N₂ to NH₃ and a silyldiazenido model intermediate†

Michael J. Dorantes, (1) ‡ James T. Moore, (1) ‡ Eckhard Bill, Bernd Mienert and Connie C. Lu (1) *

A tin-supported iron catalyst produces 5.9 turnovers of NH_3 from N_2 , using $[Ph_2NH_2]OTf$ as the acid and $CoCp_2*$ as the reductant. Two redox states of the $Fe(N_2)$ adduct and an Fe silyldiazenido complex were characterized using X-ray crystallography along with NMR and Mössbauer spectroscopies. Density functional theory calculations reveal that the charge on the Sn center correlates strongly with both the polarization of the N_2 moiety and the charge on the distal N atom.

The conversion of dinitrogen into reduced feedstocks using well-defined transition-metal catalysts has steadily advanced since Schrock and Yandulov reported the Mo triamidoamine catalyst in 2003. The development of other metal-based catalysts for N₂ fixation has led to a greater understanding of the diverse mechanisms and increasingly high catalytic turnovers. Notably, Nishibayashi and coworkers reported a Mo pincer catalyst capable of producing 4350 equiv. of NH₃ using HOCH₂. CH₂OH/SmI₂ as a coupled proton and electron source. However, these developments are weighted primarily toward early transition metals. Comparatively, the number of late-transition metal catalysts is limited, including the Fe-based catalysts (Fig. 1).

Here, we report an Fe catalyst that is largely inspired by Peters' nitrogen fixation catalyst, $P_3^{\ B}Fe^+$, $(P_3^{\ B}=tris(o\text{-}diisopropyl-phosphinophenyl)borane). In comparison to other anchoring atoms such as C and Si, Peters and coworkers have concluded that borane uniquely enhances the catalytic performance by conferring stability to the hydrazido intermediate, FeNNH₂. Using a previously reported bimetallic Fe–Sn system, we generated the <math>N_2$

‡ co-first authors

adduct, LSnFeN₂ (1), where L is the double-decker ligand, $[N(o-(NCH_2P^iPr_2)(C_6H_4)_3)]^{3-}$. Complex 1 mediates the catalytic reduction of N₂ to NH₃ with 5.9 turnovers. The properties of 1, its reduced analogue, $K(THF)_3$ ·LSnFe(N₂) (2), and the N₂-functionalized diazenido complex, LSnFeN₂SiMe₃ (3), were characterized structurally, spectroscopically, and theoretically. To the best of our knowledge, this work provides the first example of catalytic N₂ reduction that leverages a direct Fe–Sn interaction. Also, this study adds to the limited examples of Sn-supported first-row transition metal complexes.⁸

The addition of FeBr $_2$ to the metalloligand Li(THF) $_3$ -LSn in THF led to the previously reported bimetallic complex, LSnFeBr. Crystallization of LSnFeBr by Et $_2$ O diffusion into a concentrated benzene solution provided deep-red crystals in 68% yield. Next, the one- and two-electron reductions of LSnFeBr in THF under a N $_2$ atmosphere were affected by adding 1.1 equiv. and 2.2 equiv. KC $_8$, respectively, whereupon the solution changed color from red to yellow orange and then to deep orange.

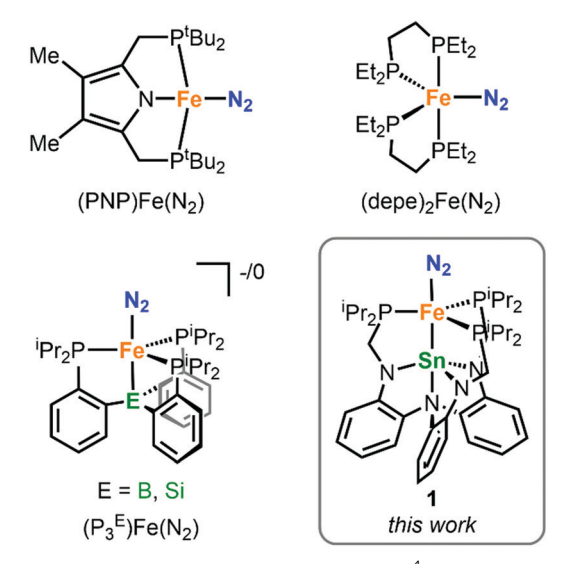


Fig. 1 Selected Fe-based catalysts for N₂ fixation.⁴

^a Department of Chemistry, University of Minnesota, 207 Pleasant Street SE, Minneapolis, Minnesota 55455-0431, USA. E-mail: clu@umn.edu

^b Max Planck Institut für Chemische Energiekonversion, Stiftstraße 34-36, 45470 Mülheim an der Ruhr, Germany

[†] Electronic supplementary information (ESI) available: Experimental details for the synthesis, spectroscopic characterization, crystallographic data, catalysis data and DFT calculations. CCDC 2007833–2007836. For ESI and crystallographic data in CIF or other electronic formats see DOI: 10.1039/d0cc04563b

Communication ChemComm

The one-electron reduced species, LSnFe(N_2) (1), is paramagnetic with an S = 1/2 ground state ($\mu_{\rm eff} = 1.87 \ \mu_{\rm B}$, Evans method). The N₂ ligand is bound in a terminal, end-on manner (vide infra). The N-N stretching frequency of 2011 cm⁻¹ (IR, KBr pellet, ESI† Fig. S11) indicates the moderate activation of the N₂ unit that is comparable to other polyphosphine Fe(N2) complexes. 9 The doubly reduced species, K(THF)3·LSnFe(N2) (2), is diamagnetic and displays a single ³¹P{¹H} NMR peak at 88.2 ppm (THF-d₈). A 119Sn NMR quartet peak was observed at 511.6 ppm, which arises from the 119Sn nucleus coupling to three equivalent ³¹P nuclei $(I = \frac{1}{2}, 100\%)$ through the Fe nucleus, with a ${}^2J_{Sn-P}$ value of 610 Hz (ESI,† Fig. S4). The ¹H₁³¹P₁ NMR spectrum with seven unique resonances is consistent with a trigonal symmetry in solution (ESI,† Fig. S2). The N-N stretching frequency for the [2.2.2]cryptand derivative, K(crypt-222)[LSnFe(N₂)], of 1944 cm⁻¹ (IR, KBr pellet, ESI,† Fig. S12), supports increased electron density at Fe, allowing for amplified backbonding into the N_2 π^* orbitals.

Single-crystal X-ray diffraction studies were performed for 1 and 2 (see the ESI†). In both structures, the Fe center is trigonal bipyramidal with an end-on N_2 ligand in the axial position trans to the Sn center (Fig. 2). The N-N bond elongates by 0.03 Å from 1.112(2) Å in 1 to 1.143(6) Å in 2 (cf. free N₂ 1.10 Å, Table S2, ESI†). The Fe-N2 bond contracts by the same magnitude, consistent with increased Fe-to- N_2 π -backbonding in 2. Notably, all the other bonds around Fe contracted upon reduction. In comparing 2 to 1, the Fe-Sn and avg Fe-P bonds are shorter by 0.03 and 0.07 Å, respectively. As an aside, the Fe-Sn bond lengths (2.4470(3) in 1 and 2.4215(8) Å in 2) are both smaller

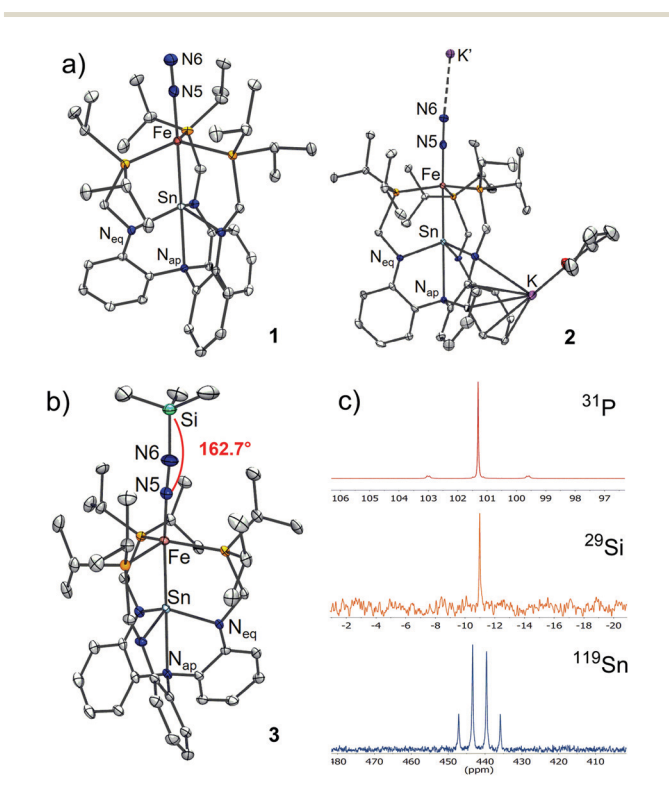


Fig. 2 (a and b) Solid-state structures of 1, 2, and 3. Thermal ellipsoids set at 50% probability with hydrogen atoms omitted. (c) $^{31}P\{^{1}H\}$, ^{29}Si , and 119 Sn NMR spectra of ${f 3}$ in THF-d $_{8}$. (See the ESI† for the full spectra.)

than the sum of their covalent radii (cf. 2.59 Å), suggesting the presence of a Fe-Sn bonding interaction. Complex 2 crystallized as a 1-D coordination polymer, where the bridging K⁺ ion is chelated by the ligand backbone of one molecule while binding the N2 ligand of another. Because of a singularly short $K-N_{eq}$ interaction, one of the $Sn-N_{eq}$ bonds is significantly elongated in 2, precluding a direct comparison of the Sn firstcoordination shell between 1 and 2.

In heterobimetallic complexes, the presence of intermetal covalent bond(s) can complicate the assignment of formal oxidation states of the individual metal centers. Adapting the Feltham–Enemark notation¹⁰ to tally the total valence electrons of the bimetal unit,11 the electronic configurations for LSnFeBr, 1, and 2 are denoted as {FeSn}⁸, {FeSn}⁹, and {FeSn}¹⁰. This redox triad was interrogated through the electrochemical study of 1 and 2. The cyclic voltammograms (ESI† Fig. S14 and S15) revealed a reversible one-electron redox event at $E_{1/2} = -1.89 \text{ V}$ vs. $FeCp_2^{+/0}$, which is assigned to the $\{FeSn\}^{9/10}$ redox couple, and an irreversible oxidation at $E_{\rm pa} \sim -0.76 \text{ V} (0.4 \text{ M} [^n \text{Bu}_4 \text{N}] [\text{PF}_6] \text{ in}$ THF). For the latter oxidation, the irreversibility is likely due to N₂ dissociation from the cationic {FeSn}⁸ species.

Starting from the {FeSn}¹⁰ species 2, N₂ functionalization was affected by using an electrophilic reagent in accordance with the previous literature. 9c Reaction of 2 with a slight excess of Me₃SiCl yielded the diazenido complex, LSnFeN₂SiMe₃ (3), as a lavender powder that is highly soluble in organic solvents ranging from pentane to THF. Structurally characterized Fe diazenido complexes that are derived from N2 are still limited in the literature. 6c,9c,12 The N-N vibration at 1756 cm⁻¹ (IR, KBr pellet, ESI,† Fig. S13) for 3 compares well with the reported values for Fe diazenido complexes (ESI,† Table S3). 9c,12a Complex 3 was characterized using a suite of heteronuclear NMR spectroscopies (Fig. 2). A downfield ³¹P{¹H} NMR resonance at 101.3 ppm was observed with satellites arising from $^2J_{\rm P-Sn}$ coupling to the $^{119}{\rm Sn}$ (natural abundance: 7.7%) and 117 Sn (8.6%) nuclei of 561 and 538 Hz, respectively. In the 119 Sn NMR spectrum, a quartet was observed at 441.5 ppm, with a matching ${}^2J_{Sn-P}$ value of 559 Hz. Compared to 2, 3 has a slightly lower ${}^{2}J_{Sn-P}$ value, which is consistent with the longer Fe-Sn bond in 3. The 29 Si NMR resonance at -11.0 ppm falls well within the range of previously reported resonances for Fe silyldiazenido complexes9c,12a

Single crystals of 3 were grown from a concentrated Et₂O solution stored at -30 °C for 48 h (Fig. 2). The structure shows that the N-N bond lengthened to 1.182(3) Å, which is intermediate between a double (1.25 Å) and triple (1.10 Å) N-N bond. The Fe-N bond contracted to 1.686(2) Å, indicative of multiple bond character. 13 The remaining bonds in the Fe firstcoordination shell are expanded in 3 relative to 2, where the avg Fe-P and Fe-Sn bonds increase by 0.04 and 0.05 Å, respectively. The N-N-Si vector has a corresponding bond angle of 162.7(3)°, a value that is between linear and bent ($\sim 130^{\circ}$). This bond angle is similar to that in $(P_3^{Si})Fe(N_2SiMe_3)$ (165.6°), but in sharp contrast to bent angles in [Fe(diphosphine)₂(N₂SiMe₃)][BAr₄^F] complexes (127°, 134°). 9c,12a Diazenido ligands, which are isoelectronic to nitrosyl ligands, are redox non-innocent, and hence,

ChemComm Communication

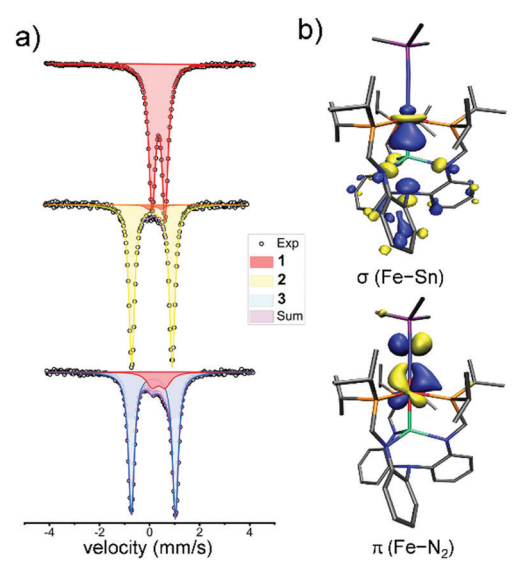


Fig. 3 (a) Zero-field ⁵⁷Fe Mössbauer spectra recorded at 80 K. Experimental data are indicated by the dotted points. In samples of 2 and 3, LSnFeN2 (1) is present as an impurity at 3% and 14%, respectively. Tabulated parameters can be found in Table S4 (ESI†). (b) DFT-calculated MOs of 3 showing the Fe-Sn σ -bond and the enhanced Fe-N₂ π -backbonding upon silylation.

metal diazenido species can be described using two limiting resonance structures: M=N=N-R and M-N=N-R.14 The former features a bent diazenido ligand (i.e. bent N-N-R angle) that is formally classified as a 3-electron, LX-donor; the latter is best described as a diazenium ligand, which akin to NO⁺ is a cationic 2-electron L-donor. Collectively, the structural parameters in 3 support bonding that is in between these two resonance forms.

Solid samples of 1, 2, and 3 were subjected to zero-field ⁵⁷Fe Mössbauer spectroscopy at 80 K. Each spectrum showed a relatively clean quadrupole doublet (Fig. 3a, Fig. S17 and Table S4, ESI†). The isomer shift (δ) steadily decreases from **1** to **2** to **3**: 0.47, 0.35, and 0.26 mm s⁻¹, respectively. The observed decrease in δ upon reduction is typical for low-valent Fe systems. ¹⁵ The lowering of δ has been attributed to the increase in the Fe 4s population that arises from greater Fe-to-L π -backbonding, or shorter, more covalent Fe-L bonds. 15a,16 In this series, the only bond that consistently contracts is the Fe-N bond (whether the ligand is N₂ or N₂SiMe₃), which decreases from 1.793(1) Å in 1 to 1.762(5) Å in 2, and then to 1.686(2) Å in 3. The quadrupole splitting ($|\Delta E_{\rm Q}|$) increases from 0.52 mm s⁻¹ in 1 to 1.62 mm s⁻¹ in 2, but only slightly increases to 1.76 mm s⁻¹ in 3. The trends in both δ and $|\Delta E_{\rm O}|$ match well to those reported for $[(P_3^{\rm Si}){\rm Fe}(N_2)]^{0/-}$ and (P_3^{Si}) Fe (N_2SiMe_3) (Table S4, ESI†). 9c,17 The δ values for 2 and 3 are different ($\Delta \delta = 0.11 \text{ mm s}^{-1}$), whereas the $|\Delta E_{\rm O}|$ values are similar. Hence, it remains unclear whether the configuration of {SnFe(N2R)}10 in 3 would be best described as an {FeSn}10 unit that π -backbonds into a silyldiazenium(1+) moiety or an {FeSn}⁸ unit with a π -donating diazenido(2–) ligand.

Density functional theory (DFT) calculations (M06-L, see the ESI† for computational details) were also performed to probe the electronic structures of 1-3. Overall, there is good agreement between the computed and experimental geometries (ESI,† Table S5). The resulting MO diagrams for 1-3 all show a

covalent Fe-Sn σ -bond, where the Sn $(5p_2, 5s)$ and Fe $(3d_z^2)$ contributions are almost equal (Fig. 3b and ESI,† Fig. S18—S20). The ground-state configurations of 1 and 2 are consistent with $(\sigma_{\text{Fe-Sn}})^2$ (Fe d_{xz} , d_{yz})⁴ (Fe d_{xy} , $d_{x^2-y^2}$)ⁿ $(\sigma_{\text{Fe-Sn}}^*)^0$, where n is 3 and 4, respectively. The MO diagram for 3 also shows highly covalent π -bonds between Fe and N₂SiR₃, and is consistent with the ground-state configuration: $(\sigma_{\text{Fe-Sn}})^2(\pi_{\text{Fe-N2}})^4(\text{Fe-d}_{xy})$ $d_{x^2-v^2}$) $^4(\pi_{Fe-N_2}^*)^0(\sigma_{Fe-S_n}^*)^0$.

To elucidate the bonding in 1-3, the Fe-N and N-N bond orders were analyzed using the density derived electrostatic and chemical (DDEC6) method. 18 This analysis revealed a gradual increase in the Fe-N bond order from 1 to 2 to 3: 1.13, 1.20, and 1.50, respectively (ESI,† Fig. S21). Simultaneously, the N-N bond order decreases from 1 to 2 to 3: 2.58, 2.56, and 2.18, respectively. Indeed, coordination of the SiMe3+ group results in a more polarized and weakened N-N bond, as reflected by the increased negative charge on the distal N-atom in 3 (-0.37) compared to 1 (-0.15) and 2 (-0.24) (ESI,† Table S9). Similar trends were observed upon the coordination of Lewis acidic boranes to the distal N of Fe(depe)₂(N_2), culminating in the selective protonation at the distal N site due to its enhanced negative charge. 12b In 1-3, the charge of the distal N and the charge difference between the N atoms were found to correlate best with the charge of Sn $(R_{adi})^2$ = 0.997 and 0.988, respectively, Fig. S23 and S24, ESI†). These strong correlations suggest that the identity of the atom trans to the N2 unit may have a substantial effect on the distal N's nucleophilicity, which would likely govern how readily the N2 unit can undergo further functionalization.

Next, we investigated the catalytic performance of 1-3 in reducing N2 to NH3. Using similar conditions to those developed by Peters and coworkers, 4b the catalyst (2.3 μmol), [Ph₂NH₂]OTf (108 equiv.), CoCp₂* (54 equiv.), and Et₂O were sealed in a vessel while under 1 atm N_2 at $-196\ ^{\circ}\text{C},$ and then stirred at -78 °C for 3 h. The Ph₂NH₂⁺ acid and the CoCp₂* reductant are proposed to initially form the protonated metallocene, Co(η⁴-Cp*H)(Cp*), which mediates the proton-coupled electron transfer during N2 reduction.5 Table 1 summarizes the results of the catalytic runs, which were performed in triplicate (ESI,† Table S10). Catalyst 1 generated 5.9(5) turnovers of NH₃ (33% yield, entry 1). Moreover, catalytic activity was retained in the presence of Hg(s) (entry 2), supporting an active species that is homogeneous. In comparison, the P₃^BFe⁺ catalyst produced 12.8 turnovers of NH₃ in a single catalytic run and reached 84 NH₃ turnovers after 3 consecutive runs (entries 5 and 6).⁵ For NH₃ production under these specific conditions, 1 is half as active as P₃^BFe⁺ in a single catalytic run, and outperforms both $P_3^{Si}Fe(N_2)^5$ and $Fe(depe)_2(N_2)^{12a}$ five-fold (entries 7 and 8). We note that other Fe catalysts require harsher reagents such as $H(Et_2O)_2B(Ar^F)_4$ and KC_8 to mediate N_2 to NH_3 . $^{4c-e,19a,b}$

The N2 reduction reaction, however, was rendered substoichiometric when 2 was used as the catalyst (entry 3), presumably due to the low solubility of 2 in Et₂O. On the other hand, catalyst 3 gave comparable turnovers (entry 4) as 1, supporting the ability of a metal silyldiazenido species to enter the N₂ reduction cycle. Because metal silyldiazenido species are proposed as intermediates in catalytic N2 silylation, we also tested 3 for N2 Communication ChemComm

Table 1 Results of catalytic reduction of dinitrogen to ammonia using Fe–Sn complexes (1-3) and comparisons to known Fe catalysts

No +	CoCn*a	. +	[Ph ₂ NH ₂]OTf	Fe catalyst	NHa
2	x equiv	-		Et ₂ O, -78 °C, 3 h	•
ntry Cata	lyst	x (ec	uiv.) γ (equiv.) Ν	NH3 turnovers Yield ^a	(%) Re

Entry	Catalyst	x (equiv.)	y (equiv.)	NH ₃ turnovers	$Yield^a$ (%)	Ref.
1	1	54	108	5.9(5)	33	_
2	1 + $Hg_{(s)}^{b}$	54	108	5.2(8)	29	_
3	2	54	108	0.8(5)	5	_
4	3	54	108	4.6(2)	26	_
5	$P_3^B Fe^+$	54	108	12.8(5)	72	4b
6	$P_3^B Fe^+$	162×3^c	322×3^c	84(8)	52	4b
7	$P_3^{Si}Fe(N_2)$	54	108	1.2(1)	7	4b
8	$(depe)_2 Fe(N_2)$	54	108	$1.1(2)^d$	6	4 <i>g</i>

 $[^]a$ Yield is based on the reductant. b 200 equiv. Hg was added to the reaction vessel before the start of catalysis. c In each of the 3 cycles, the reaction was cooled to $-196~^{\circ}\mathrm{C}$ to replenish the reagents and solvents. d (depe) $_2\mathrm{Fe}(N_2)$ is selective for hydrazine with 8.9(1) equiv. N_2H_4 in addition to 1.1(2) equiv. NH_3 .

silylation using Me₃SiCl and KC₈ as the added reagents. Disappointingly, 3 only generated 1.2 equiv. of N(SiMe₃)₃, which is relatively poor compared to other reported systems.^{2b}

In summary, a family of Fe-Sn bimetallic complexes has enabled the characterization and comparison of a series of nitrogen fixation catalysts, capable of generating ammonia in up to 5.9 equivalents. Experimental and computational results together show a clear and comparable trend of increased N2 activation evidenced by decreased N2 bond order, stretching frequency, and increased negative charge on the distal nitrogen upon reduction from 1 to 2, and even more so in the silvlation of 2 to 3. For all of these complexes, a direct Fe-Sn covalent interaction was present, and a linear trend was found between the charge on Sn and the charge on the distal nitrogen in the N2 moiety. This points to another potential impact of the supporting atom trans to the N₂ moiety on N₂ functionalization. Under the same catalytic conditions, the Fe-Sn bimetallic catalyst compares well with Peters' Fe-E systems, outperforming E = Si and C, but is less active than E = B. This type of comparison lends additional understanding into the factors that generate active Fe-E catalysts. Additional studies with different supporting atoms and further functionalization of the presented complexes are currently underway.

The authors thank the NSF (CHE-1800110) for support and Dr Victor G. Young, Jr. (CHE-1229400) for X-ray crystallography.

Conflicts of interest

There are no conflicts to declare.

Notes and references

- 1 D. V. Yandulov and R. R. Schrock, Science, 2003, 301, 76-78.
- (a) D. Singh, W. R. Buratto, J. F. Torres and L. J. Murray, *Chem. Rev.*, 2020, 120, 5517–5581; (b) S. Kim, F. Loose and P. J. Chirik, *Chem. Rev.*, 2020, 120, 5637–5681; (c) M. J. Chalkley, M. W. Drover and J. C. Peters, *Chem. Rev.*, 2020, 120, 5582–5636.
- 3 Y. Ashida, K. Arashiba, K. Nakajima and Y. Nishibayashi, *Nature*, 2019, 568, 536–540.
- 4 (a) J. Higuchi, S. Kuriyama, A. Eizawa, K. Arashiba, K. Nakajima and Y. Nishibayashi, *Dalton Trans.*, 2018, 47, 1117–1121; (b) M. J. Chalkley, T. J. Del Castillo, B. D. Matson and J. C. Peters, *J. Am. Chem. Soc.*, 2018, 140, 6122–6129; (c) R. Imayoshi, K. Nakajima, J. Takaya, N. Iwasawa and Y. Nishibayashi, *Eur. J. Inorg. Chem.*, 2017, 3769–3778; (d) S. Kuriyama, K. Arashiba, K. Nakajima, Y. Matsuo, H. Tanaka, K. Ishii, K. Yoshizawa and Y. Nishibayashi, *Nat. Commun.*, 2016, 7, 12181; (e) S. E. Creutz and J. C. Peters, *J. Am. Chem. Soc.*, 2014, 136, 1105–1115; (f) Y. Sekiguchi, S. Kuriyama, A. Eizawa, K. Arashiba, K. Nakajima and Y. Nishibayashi, *Chem. Commun.*, 2017, 53, 12040–12043; (g) P. J. Hill, L. R. Doyle, A. D. Crawford, W. K. Myers and A. E. Ashley, *J. Am. Chem. Soc.*, 2016, 138, 13521–13524; (h) J. S. Anderson, J. Rittle and J. C. Peters, *Nature*, 2013, 501, 84–87.
- 5 M. J. Chalkley, T. J. Del Castillo, B. D. Matson, J. P. Roddy and J. C. Peters, ACS Cent. Sci., 2017, 3, 217–223.
- 6 (a) B. D. Matson and J. C. Peters, ACS Catal., 2018, 8, 1448–1455;
 (b) M. M. Deegan and J. C. Peters, Chem. Sci., 2018, 9, 6264–6270;
 (c) J. Rittle and J. C. Peters, J. Am. Chem. Soc., 2016, 138, 4243–4248.
- 7 S. C. Coste, B. Vlaisavljevich and D. E. Freedman, *Inorg. Chem.*, 2017, 56, 8195–8202.
- 8 D. Das, S. S. Mohapatra and S. Roy, Chem. Soc. Rev., 2015, 44, 3666–3690.
- (a) J. S. Anderson, M. E. Moret and J. C. Peters, J. Am. Chem. Soc.,
 2013, 135, 534–537; (b) L. R. Doyle, P. J. Hill, G. G. Wildgoose and
 A. E. Ashley, Dalton Trans., 2016, 45, 7550–7554; (c) Y. Lee,
 N. P. Mankad and J. C. Peters, Nat. Chem., 2010, 2, 558–565;
 (d) M. E. Moret and J. C. Peters, J. Am. Chem. Soc., 2011, 133, 18118–18121.
- 10 J. H. Enemark and R. D. Feltham, Coord. Chem. Rev., 1974, 13, 339-406.
- 11 (a) B. Wu, M. J. Wilding, S. Kuppuswamy, M. W. Bezpalko, B. M. Foxman and C. M. Thomas, *Inorg. Chem.*, 2016, 55, 12137–12148; (b) R. J. Eisenhart, P. A. Rudd, N. Planas, D. W. Boyce, R. K. Carlson, W. B. Tolman, E. Bill, L. Gagliardi and C. C. Lu, *Inorg. Chem.*, 2015, 54, 7579–7592.
- 12 (a) A. D. Piascik, P. J. Hill, A. D. Crawford, L. R. Doyle, J. C. Green and A. E. Ashley, *Chem. Commun.*, 2017, 53, 7657–7660; (b) J. B. Geri, J. P. Shanahan and N. K. Szymczak, *J. Am. Chem. Soc.*, 2017, 139, 5952–5956.
- 13 P. L. Holland, Dalton Trans., 2010, 39, 5415-5425.
- 14 J. R. Dilworth, Coord. Chem. Rev., 2017, 330, 53-94.
- (a) F. Neese, Inorg. Chim. Acta, 2002, 337, 181–192; (b) P. Gutlich,
 E. Bill and A. X. Trautwein, Mössbauer Spectroscopy and Transition Metal Chemistry, Springer, 2011.
- 16 J. T. Moore, S. Chatterjee, M. Tarrago, L. J. Clouston, S. Sproules, E. Bill, V. Bernales, L. Gagliardi, S. Ye, K. M. Lancaster and C. C. Lu, *Inorg. Chem.*, 2019, 58, 6199–6214.
- 17 P. A. Rudd, N. Planas, E. Bill, L. Gagliardi and C. C. Lu, Eur. J. Inorg. Chem., 2013, 3898–3906.
- (a) N. G. Limas and T. A. Manz, RSC Adv., 2018, 8, 2678-2707;
 (b) T. A. Manz, RSC Adv., 2017, 7, 45552-45581.
- (a) Y. Nishibayashi, *Dalton Trans.*, 2018, 47, 11290–11297;
 (b) T. J. Del Castillo, N. B. Thompson and J. C. Peters, *J. Am. Chem. Soc.*, 2016, 138, 5341–5350.